buildings

Article

Dynamic Response and Impact Force Calculation of PC Box Girder Bridge Subjected to Over-Height Vehicle Collision

Yuan Jing [1,*], Xu Zhang [1], Yongjun Zhou [1], Yu Zhao [1] and Wenchao Li [2]

[1] School of Highway, Chang'an University, Xi'an 710064, China
[2] School of Civil Engineering, Chang'an University, Xi'an 710061, China
* Correspondence: yjing@chd.edu.cn

Abstract: The dynamic response of a prestressed concrete box girder bridge under the impact of an over-height vehicle is studied using the numerical simulation method. The finite element analysis software LS-DYNA is used to simulate the collision between the bridge superstructure and an over-height truck. Further, a parametric analysis is carried out to investigate the influence of six factors, i.e., girder configuration, vehicle speed, vehicle mass, impact angle, concrete strength and strand prestress, on both local damage and overall performance of the bridge. The numerical analysis results show that the girder configuration, vehicle speed, vehicle mass and impact angle have obvious effects on both local damage and the overall behavior of the PC box girder bridge. Whereas, the concrete strength and strand prestress only have a certain effect on the local damage at the impact area with very limited influence on the overall behavior of the bridge. In addition, based on the results obtained from the numerical simulation and parametric analysis, a formula for predicting the peak and average impact force of the prestressed concrete box girder bridge under the over-height vehicle impact is developed. The proposed impact force formula comprehensively accounts for the influence of the vehicle speed, vehicle mass and impact angle and can accurately predict the impact force generated under different working conditions, which confirms the promising prospect of the proposed formula in practical applications.

Keywords: bridge engineering; prestressed concrete box girder bridge; over-height vehicle; dynamic response; impact force calculation

Citation: Jing, Y.; Zhang, X.; Zhou, Y.; Zhao, Y.; Li, W. Dynamic Response and Impact Force Calculation of PC Box Girder Bridge Subjected to Over-Height Vehicle Collision. *Buildings* **2023**, *13*, 495. https://doi.org/10.3390/buildings13020495

Academic Editor: Eva O.L. Lantsoght

Received: 13 January 2023
Revised: 8 February 2023
Accepted: 9 February 2023
Published: 11 February 2023

1. Introduction

Over-height vehicle impact is one of the major factors causing damage to or even collapse of bridges. Many surveys show that accidents of over-height vehicle collisions on bridges are experiencing a significant increase across the world. It is reported that more than half of the bridge superstructures in Beijing, China, were threatened by the impact of over-height vehicles [1], and around 20% of the damaged bridges in Beijing are induced by over-height vehicle collisions [2]. The United Kingdom Department of Transport reported that the number of over-height vehicle collisions at railway bridges increased from 729 to 1870 during the period of 1990–1994 [3]. Further, a survey from the Texas Department of Transportation in the United States revealed that the number of accidents of over-height vehicle impact on overpasses increased stably from 1987 to 1992, with 14% of the investigated bridges experiencing serious damage on the bridge girder [4]. In the meantime, the frequency of over-height vehicle collisions on bridge superstructures in Maryland increased by 81% from 1995 to 2000 [5]. This type of over-height vehicle collision accident not only threatens the safety of the bridge but also causes certain economic losses and casualties, which has raised great concern in the engineering field.

The dynamic behaviors and failure modes of the concrete beams under impact loading have been studied through small-scale impact tests or finite element simulations in recent years [6–12]. Fujikake et al. [6] carried out drop-weight impact tests on the reinforced concrete (RC) beams by releasing a steel hammer from different heights. The experimental result shows that the failure mode of the RC beam is strongly controlled by the drop height of the hammer. Kishi et al. [7] conducted a falling weight impact test on 27 simply supported RC beams without shear rebars, where the test results illustrated that the RC beams failed in a shear mode when the static shear-bending capacity ratio was less than 1.0. Jin et al. [8] studied the influence of different combinations of impact mass and velocity on the dynamic response of RC beams by establishing a three-dimensional meso numerical model. It was found that with the increase of impact impulse, the failure mode of reinforced concrete beams changes from shear failure to bending failure, and the energy dissipation of reinforcement and the whole member increases. Xu et al. [9] carried out small-scale pendulum impact tests on different types of girders and the test results implied that the girder configuration controlled the failure mode of the above component, where a global failure was obtained for the steel box girder, whereas a local failure was obtained for the steel plate and RC T-shaped girder. Jing et al. [10] carried out a full-scale lateral impact test on a prestressed concrete (PC) girder by releasing a rigid impact cart from a certain height. The experiment shows that both a serious overall failure and local damage occurred on the PC box girder, which confirms the threat of the over-height vehicle collision on the safety of the bridge. For the bridge superstructure, the finite element analysis method is generally used to investigate its dynamic responses and damage mechanism [13–16]. Yang et al. [13] studied the lateral impact resistance of a prestressed concrete beam bridge by conducting finite element simulation. In the study, the influence of several key parameters was investigated and the results showed that the use of the diaphragm would significantly enhance the impact resistance of prestressed concrete beam bridges. Zhang et al. [14] conducted a refined finite element simulation on a PC box girder bridge impacted by falling objects. The dynamic response and damage mechanism were explored by changing the impact parameters and the residual bearing capacity of the impacted girder was evaluated as well. Cao et al. [15] performed a computational study of the Skagit River bridge collapse under an over-height tractor–semitrailer impact. The characteristic of the impact force and the collapse mechanism of the bridge were investigated and a protection beam was suggested to be used to mitigate the risk from the over-height vehicles.

In addition, for the design of the superstructure to resist vehicle collision, the impact force is an intuitive factor to indicate the intensity of the vehicular impact, once it is determined, the structural analysis and damage evaluation can be conducted. Current specifications provide very limited methods to estimate the impact force transferred to the bridge structures during the vehicle collision. The General Specifications for Design of Highway Bridges and Culverts (JTG D60-2015) in China [17] and AASHTO LRFD Bridge Design Specification [18] specify the magnitude and location of the equivalent impact force generated from the vehicle impact; however, both are for the bridge substructure. The European Code (Eurocode EN1991-1-7) [19] provides a simple design provision, where a value of 500 kN is specified as the equivalent static design force for the superstructure of the bridge subjected to a vehicle collision. This equivalent static design force is derived from the hard impact which, thus, does not account for the characteristics of both vehicle and bridge superstructures. In order to solve the above problems, a few studies were performed to calculate the impact force of the bridge superstructure. Xu et al. [20] conducted a finite element analysis on the vehicle-bridge collision and proposed a simplified calculation model for the impact between over-height vehicles and the bridge superstructure by simplifying the influence parameters and making a series of assumptions. Based on this simplified calculation model, the impact force calculation equations were proposed. Liu et al. [21] established a refined finite element model using LS-DYNA. The peak impact force of the bridge superstructure was explored by changing the vehicle mass and vehicle speed. Based on a large number of data fitting analyses, the calculation formula of impact force related to vehicle mass and vehicle speed was obtained. Kong et al. [22] investigated the damage process and collision force of PC box girder bridge under over-height vehicle impact through FE simulation. The results showed that the vehicle velocity and carriage thickness have an important effect on the peak value of the impact force, while the average impact force is mainly influenced by vehicle mass and velocity, impact height and thickness of carriage. Oppong et al. [23] studied the influences of different types of impacting objects on the bridge superstructure through a refined FE model and developed a set of equations to predict the impact force as a function of impact velocity, impact area and dimension of the impacting object.

Despite a certain amount of studies have been conducted on the structural members under impact loading, the systematic study of the bridge superstructure under over-height vehicle collision still needs to be performed to better understand the damage mechanism. In addition, the determination of the impact force during the collision is essential to understand the dynamic behavior of the structure, which also needs further investigation. In this study, the dynamic response and damage mechanism of a prestressed concrete box girder bridge under the impact of an over-height vehicle are studied by using the finite element analysis software LS-DYNA. A parametric analysis is conducted to investigate the effects of different influence factors, i.e., girder configuration, vehicle speed, vehicle mass, impact angle, concrete strength and strand prestress, on both local damage and the overall performance of the bridge. Further, a formula for predicting the peak and average impact force of the prestressed concrete box girder bridge under the impact of the over-height vehicle is developed based on the results obtained from the numerical simulation and parametric analysis. The proposed impact force formula comprehensively accounts for the influence of the vehicle speed, vehicle mass and impact angle, which can be used as an effective tool for the impact design of bridge superstructure.

2. Numerical Simulation of the Collision between an Over-Height Vehicle and a PC Box Girder Bridge

2.1. Finite Element Model of the PC Box Girder Bridge

The superstructure of a typical prestressed concrete box bridge is adopted in the vehicle-bridge collision analysis. The geometry and dimensions of the investigated bridge superstructure are illustrated in Figure 1a. As shown in Figure 1a, the investigated bridge is composed of three box girders with the span and width of the bridge deck being 20 m and 10 m, respectively. The thickness of the top flange, bottom flange and web for the box girder is 18 cm. A C50 grade concrete (i.e., the compressive strength of concrete obtained from a standard cubic specimen is 50 MPa) is adopted to form the main body of the three girders. Low relaxation high-strength steel strand with a nominal diameter of 15.24 mm is used as the prestressed strand, and the ultimate tensile strength of the strand is 1860 MPa. Two types of reinforcements HRB335 and R235 are used in the girder. The diameters of the longitudinal bars at the top flange, bottom flange and web are 22 mm and 25 mm. 8 mm and 12 mm rebars are used as stirrups with a distance of 150 mm. The detailed arrangement of the above reinforcements of the PC box girder bridge is presented in Figure 1b.

The finite element model of the above prestressed concrete box bridge is established using the FE software LS-DYNA [24]. Figure 1a,b shows the finite element model of the superstructure, where the concrete part and bearing of the bridge are modeled by 8-node single-point integration solid elements SOLID164 (with the minimum element size being 50 mm) and the prestressed strand and steel bars are modeled by the beam element BEAM161 (with the average mesh size being 120 mm).

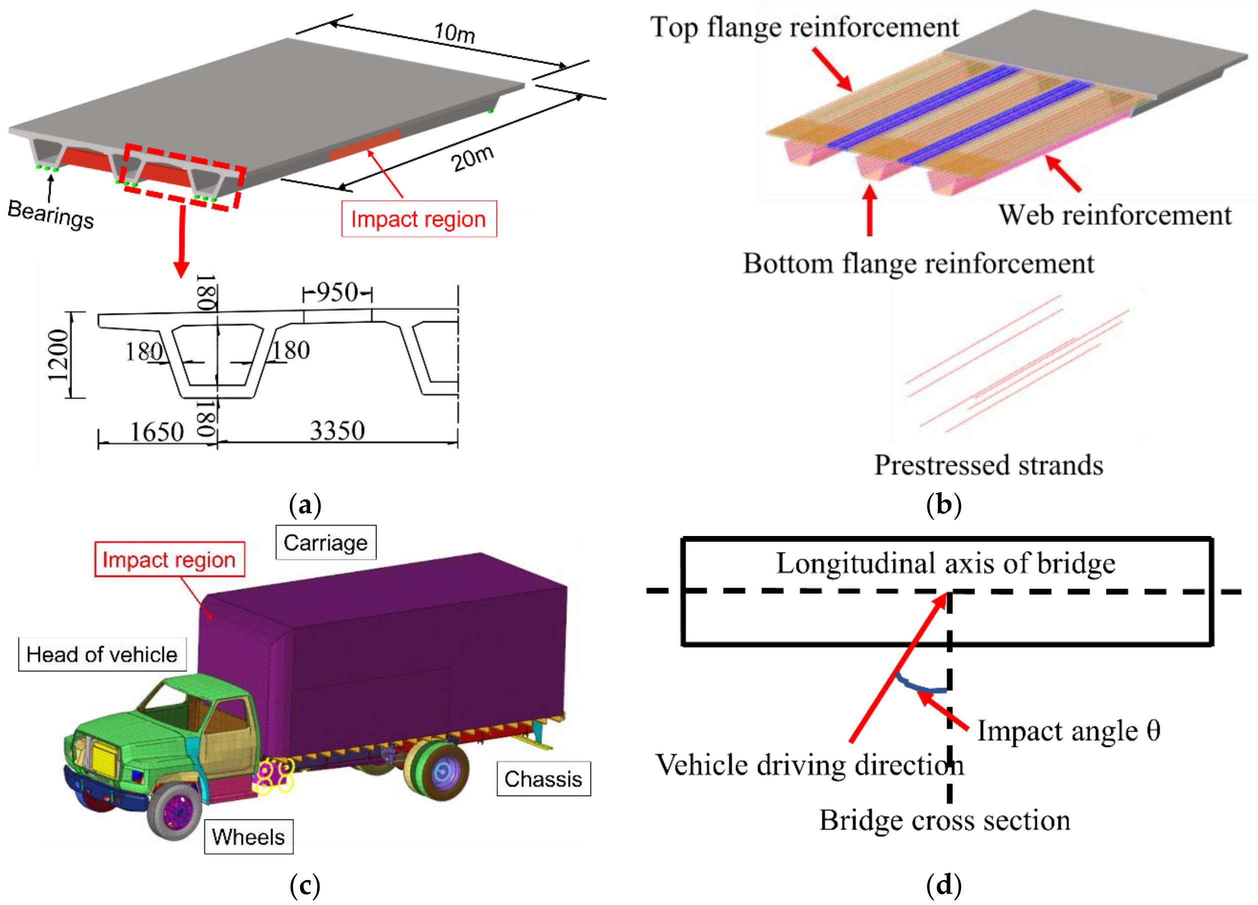

Figure 1. (**a**) Geometry and dimension of the superstructure of a PC box girder bridge. (**b**) Finite element of the PC box girder bridge. (**c**) Finite element of the over-height vehicle. (**d**) Illustration of the impact angle of the over-height vehicle.

Further, to correctly reflect the dynamic response of the superstructure, the MAT159 constitutive model (i.e., the continuous smooth cap model, * MAT_ CSCM_CONCRETE) provided in the LS-DYNA was adopted to simulate the mechanical behavior of the concrete. The strength of concrete is typically enhanced by considering the strain rate effect, where the dynamic increased factor on the strength of concrete is given in the following Equations (1)–(4) [25,26].

$$\mathrm{CDIF} = f_{cd}/f_{cs} = (\dot{\varepsilon}_d/\dot{\varepsilon}_{cs})^{1.026a} \text{ for } \dot{\varepsilon}_d \leq 30\mathrm{s}^{-1} \quad (1)$$

$$\mathrm{CDIF} = f_{cd}/f_{cs} = \gamma(\dot{\varepsilon}_d/\dot{\varepsilon}_{cs})^{1/3} \text{ for } \dot{\varepsilon}_d > 30\mathrm{s}^{-1} \quad (2)$$

$$\mathrm{TDIF} = f_{td}/f_{ts} = (\dot{\varepsilon}_d/\dot{\varepsilon}_{ts})^{\delta} \text{ for } \dot{\varepsilon}_d \leq 1\mathrm{s}^{-1} \quad (3)$$

$$\mathrm{TDIF} = f_{td}/f_{ts} = \beta(\dot{\varepsilon}_d/\dot{\varepsilon}_{ts})^{1/3} \text{ for } \dot{\varepsilon}_d > 1\mathrm{s}^{-1} \quad (4)$$

where CDIF and TDIF refer to the compressive and tensile dynamic increase factor, f_{cd} is the dynamic compressive strength at the strain rate $\dot{\varepsilon}_d$, f_{cs} is the static compressive strength at the strain rate $\dot{\varepsilon}_{cs}$, f_{td} is the dynamic tensile strength at the strain rate $\dot{\varepsilon}_d$, f_{ts} is the static tensile strength at the strain rate $\dot{\varepsilon}_{ts}$. The values for corresponding parameters are $\dot{\varepsilon}_{cs} = 30 \times 10^{-6}\mathrm{s}^{-1}$, $\dot{\varepsilon}_{ts} = 3 \times 10^{-6}\mathrm{s}^{-1}$, f_{c0} = 10 MPa, logγ = 6.156α−2, α = (5 + 9$f_{cs}/f_{c0})^{-1}$, logβ = 7.11δ−2.33, δ = 1/(10 + 6f_{cs}/f_{c0}).

In addition, the MAT3 constitutive model combined with the elastoplastic hardening material property (* MAT_PLASTIC_KINEMATIC) is adopted for the longitudinal bars and stirrups. The Cowper–Symonds model is used to account for the relationship between strain rate and tensile and compressive strength of the reinforcement. The yield stress of reinforcement and the plastic hardening modulus can be calculated according to Equations (5) and (6).

$$\sigma_{\mathrm{y}} = [1 + \left(\frac{\dot{\varepsilon}}{C}\right)^{\frac{1}{P}}](\sigma_0 + \eta E_p \varepsilon_{eff}^{p}) \tag{5}$$

$$E_p = \frac{E_t E}{E - E_t} \tag{6}$$

where σ_{y} is the yield stress of the steel rebars, $\dot{\varepsilon}$ is the strain rate of the reinforcement, C and P are the strain rate coefficients in the Cowper–Symonds model, σ_0 is the initial yield stress of reinforcement, η is a parameter used to adjust equivalent strengthening and follow-up strengthening where η = 1 means equivalent strengthening and η = 0 means follow-up strengthening,ε_{eff}^{p} is the equivalent plastic strain of the reinforcement, E_p is the plastic hardening modulus, E is the young's modulus of reinforcement, E_t is the tangent modulus.

The material property of the prestressed strand was modeled by using the material model MAT4 via the keyword * MAT_ELASTIC_PLASTIC_THERMAL. A so-called equivalent cooling method was used to apply the prestress on the strand [27]. This method assumes that the stress generated from the shrinkage process of prestressed reinforcement is equivalent to stress generated from a cooling process. Thus, we can apply a temperature change on the stand to realize the application of the prestress. The equivalent relationship between the temperature and preload on the strand can be calculated via the following equation:

$$\Delta T = \frac{N}{\varphi E A} \tag{7}$$

where ΔT is the cooling temperature value to be applied, N is the effective preload applied on the prestressed strand, A is the cross-sectional area of the prestressed strand, φ is the linear expansion coefficient of the prestressed strand, E is Young's modulus of the prestressed strand. The application of prestressed load was realized by defining the keyword of activation coupling analysis * LOAD-THERMAL-LOAD-CURVE.

Finally, the bonding relationship between the concrete and reinforcements is simulated by using the keyword * CONSTRAINED_LAGRANGE_IN_SOLID. This constraint does not consider the slip between the two materials. The bridge is simply supported and the bearings are modeled with SOLID164 element. Elastic material MAT20 is used to simulate the bearing. The translational and rotational degree-of-freedom of the nodes at the bottom surface of the bearing are constrained. Further, the investigated superstructure is simply supported. The bearings used underneath the girder are laminated rubber bearings. All the detailed material parameter values used for the analysis can be found in Table 1.

2.2. Finite Element Model of the Over-Height Vehicle

A finite element model of a Ford truck F800, provided by the National Crash Analysis Center (NCAC) of the United States [28], was adopted for the impact analysis. This vehicle model has been validated through crash tests and is widely used for the study of structural behavior under vehicle collision [29–31]. Figure 1c shows the finite element of this vehicle, where the total length, maximum width and wheelbase of the vehicle are equal to 8.54 m, 2.44 m and 5.29 m, respectively. The original self-weight of this vehicle is 7.17 tons. This weight will be changed in the following parametric analysis (see Section 3) to investigate its influence on the dynamic response of the bridge. The investigated vehicle is mainly composed of five parts: i.e., head of the vehicle, carriage, wheels, engine and chassis. Since this study mainly investigates the impact problem between the over-height vehicle and the bridge, only the carriage of the vehicle will collide with the bridge superstructure (see Figure 1c). In the numerical analysis, the * MAT_PIECEWISE_LINEAR_PLASTICITY model, which accounts for the strain rate effect, is adopted to simulate the material behavior of the carriage. Further, to obtain an accurate numerical result, a fine mesh size (50 mm) is adopted for the impact area of the vehicles. The detailed values of the material parameters of the vehicle are given in Table 1.

Table 1. Material parameters used in the numerical analysis.

Component	Material Model	Material Parameters	Values
Concrete	MAT159	Density Unconfined compression strength Maximum aggregate size Strain rate influence ERODE	2500 kg/m^3 32.35 MPa 10 mm 1 (consider) 1.05
Steel rebars	MAT3	Density Diameter Young's modulus E Tangent modulus E_t Yield strength σ_0 Poisson's ratio Strain rate coefficient C Strain rate coefficient P Equivalent plastic strain at failure	7850 kg/m^3 8 mm, 12 mm, 22 mm, 25 mm 210,000 MPa 2100 MPa 235 MPa 0.3 40.4 5 0.12
Prestressed strand	MAT4	Density Diameter Ultimate strength Applied temperature Linear expansion coefficient Poisson's ratio	8050 kg/m^3 15.24 mm 1860 MPa −484 °C 1.05×10^{-5} 0.3
Bearing	MAT20	Density Poisson's ratio Young's modulus E	7850 kg/m^3 0.3 210,000 MPa
Carriage	MAT24	Density Poisson's ratio Young's modulus E Yield strength of carriage	7850 kg/m^3 0.3 205,000 MPa 155 MPa

2.3. Collison Analysis Setting

The collision analysis for the over-height vehicle and the superstructure of the prestressed concrete box girder bridge is divided into two stages: (1) Stage 1-initial loading stage: in this stage, the gravity and prestress load of the bridge was applied on the corresponding model within 2 s. (2) Stage 2-collision stage: in this stage, a full restart function in LS-DYNA was used via the keyword * STRESS_INITIALIZATION to inherit the stress and deformation obtained from the first stage to the second stage. Then, an initial velocity was employed by the model of the vehicle to impact the superstructure of the bridge. According to the suggestion in Eurocode in Ref. [19], the vehicle was set to crash laterally at the midspan region of the concrete girder with the height of the impact region being 250 mm (see Figure 1a). The angle between the driving direction of the vehicle and the cross-section of the bridge is defined as the impact angle (see Figure 1d).

Further, to correctly simulate the contact behavior during the collision process, the AUTOMATIC_SURFACE_TO_SURFACE contact properties were employed at the interfaces between the girder and the bearings and that between the vehicle and the girder. The dynamic and static friction coefficients at all contact surfaces are set as 0.3 [32]. Further, it should be noted when the reduced integral element is used in the numerical analysis, a rigid hourglass control theory should be used to prevent the zero energy mode of these elements. According to Ref. [33], the hourglass coefficient for the elements of the concrete part of the bridge is taken as 0.05.

3. Parametric Study on the Dynamic Responses of PC Box Girder Bridge under the Impact of Over-Height Vehicle

The impact process between a bridge and an over-height vehicle is a complex nonlinear dynamic problem, which is affected by a series of factors. In this section, a parametric study is conducted to investigate the effects of different factors on the dynamic response of the prestressed concrete bridge. Six factors, including girder configuration, vehicle speed, vehicle mass, impact angle, concrete strength and prestress of the strand, are varied one by one to explore their influence on the dynamic behavior of the bridge. Further, three aspects of behaviors of the bridge, i.e., failure mode, impact force and displacement at the midspan of the bridge, are quantitatively investigated in the parametric analysis. The benchmark working condition adopted in the analysis is as follows: vehicle speed is 80 km/h, vehicle mass is 20 tons, impact angle is 0°, concrete strength is C50, and ultimate tensile strength of prestressed strand is 1860 MPa (the prestress acted on the strand is 0.75 times the ultimate tensile strength). Other investigated working conditions can be obtained from the benchmark working condition by changing the value of a single factor each time. All detailed working conditions investigated in the parametric analysis are given in Table 2.

Table 2. Working conditions investigated in the parametric analysis.

Condition	Girder Configuration	Vehicle Speed (km/h)	Vehicle Mass (t)	Impact Angle (°)	Concrete Strength	Ultimate Tensile Strength of Strand (MPa)
1	Box girder	80	20	0	C50	1860
2	Hollow slab	80	20	0	C50	1860
3	T-shaped girder	80	20	0	C50	1860
4	Box girder	40	20	0	C50	1860
5	Box girder	60	20	0	C50	1860
6	Box girder	80	10	0	C50	1860
7	Box girder	80	30	0	C50	1860
8	Box girder	80	20	15	C50	1860
9	Box girder	80	20	30	C50	1860
10	Box girder	80	20	0	C40	1860
11	Box girder	80	20	0	C60	1860
12	Box girder	80	20	0	C50	1570
13	Box girder	80	20	0	C50	1270

3.1. Influence of the Girder Configuration on the Dynamic Behavior of the Bridge

The influence of the girder configuration on the dynamic response of the bridge is investigated in this section. Despite the box girder bridge investigated in the benchmark condition, another two types of girders, i.e., the T-shaped girder and hollow slab, are also studied here. Figures 2 and 3 show the geometry and dimension of the cross-section of the investigated T-shaped and hollow slab girder. The corresponding finite element models of these types of bridges are illustrated in Figures 2 and 3 as well. The T-shaped girder bridge consists of five T-beams with three prestressed strands (having a diameter of 15.24 mm and an ultimate tensile strength of 1860 MPa) embedded in each girder. The hollow slab bridge is composed of six hollow slabs, where the side beam is reinforced with 17 prestressed strands (the same strand used in the T-shaped girder), and the middle girder is reinforced with 12 prestressed strands. In the numerical analysis, the material properties, bearings and boundary conditions of the T-shaped girder and hollow slab bridges are the same as that of the box girder bridge.

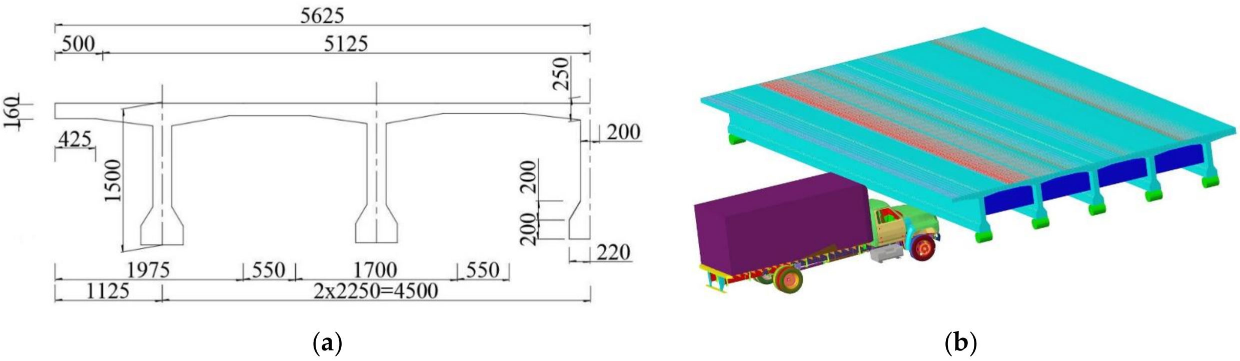

Figure 2. (**a**) Geometry and dimension of the cross-section of the T-shaped girder bridge; (**b**) finite element model of the T-shaped girder bridge.

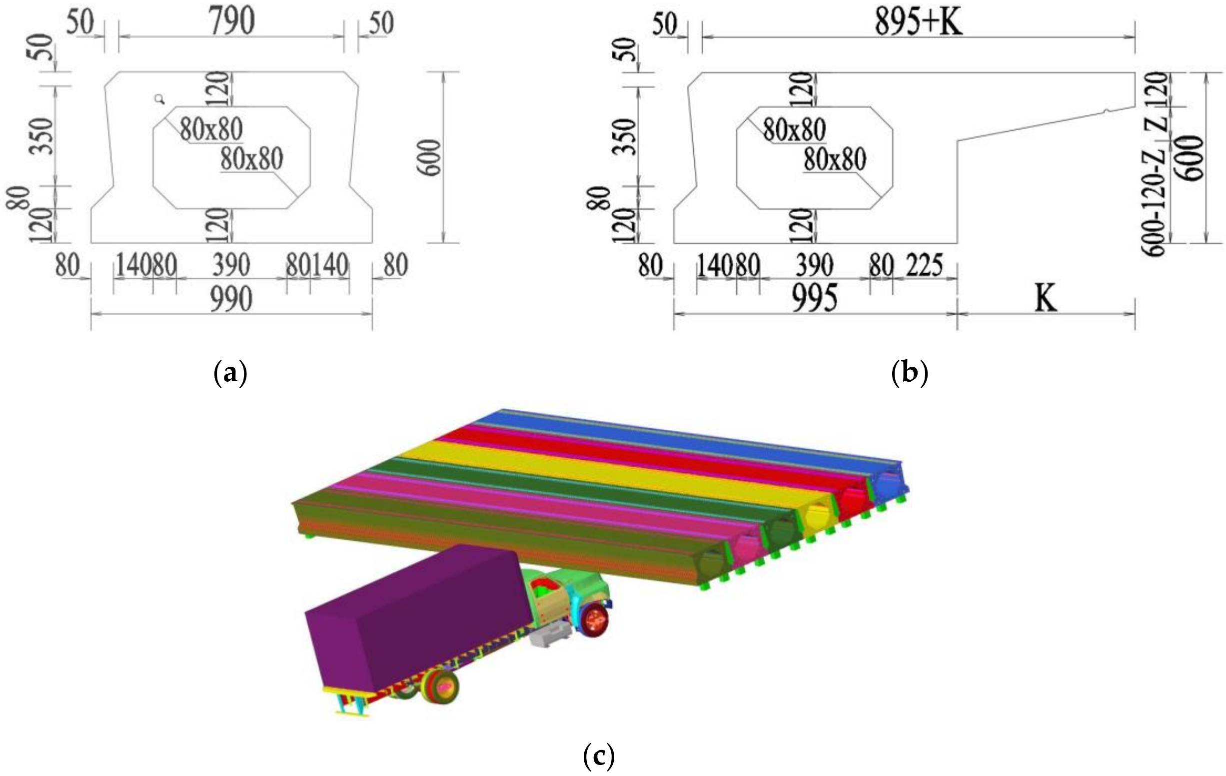

Figure 3. (**a**) Geometry and dimension of the cross-section of the middle hollow slab girder. (**b**) Geometry and dimension of the cross-section of the side hollow slab girder. (**c**) Finite element model of the hollow slab girder bridge.

(1) Failure modes of three types of bridges under impact

Figure 4 shows the effective plastic strain distribution on the three types of bridges after being impacted by a 20-ton vehicle at the midspan of the girder with the vehicle speed being 80 km/h. The damage degree of the bridge can be directly evaluated by the size of the plastic strain area and the number of deleted elements in the impact region. According to the result in Figure 4a, one can find the plastic damage on the prestressed concrete box girder bridge is minimum. The effective plastic strain mainly concentrates at the impact area of the side girder. It is found in the analysis that a large amount of concrete on the web and bottom flange of the impacted girder fell off, but the steel bars and stirrups in the impact area of the girder did not yield.

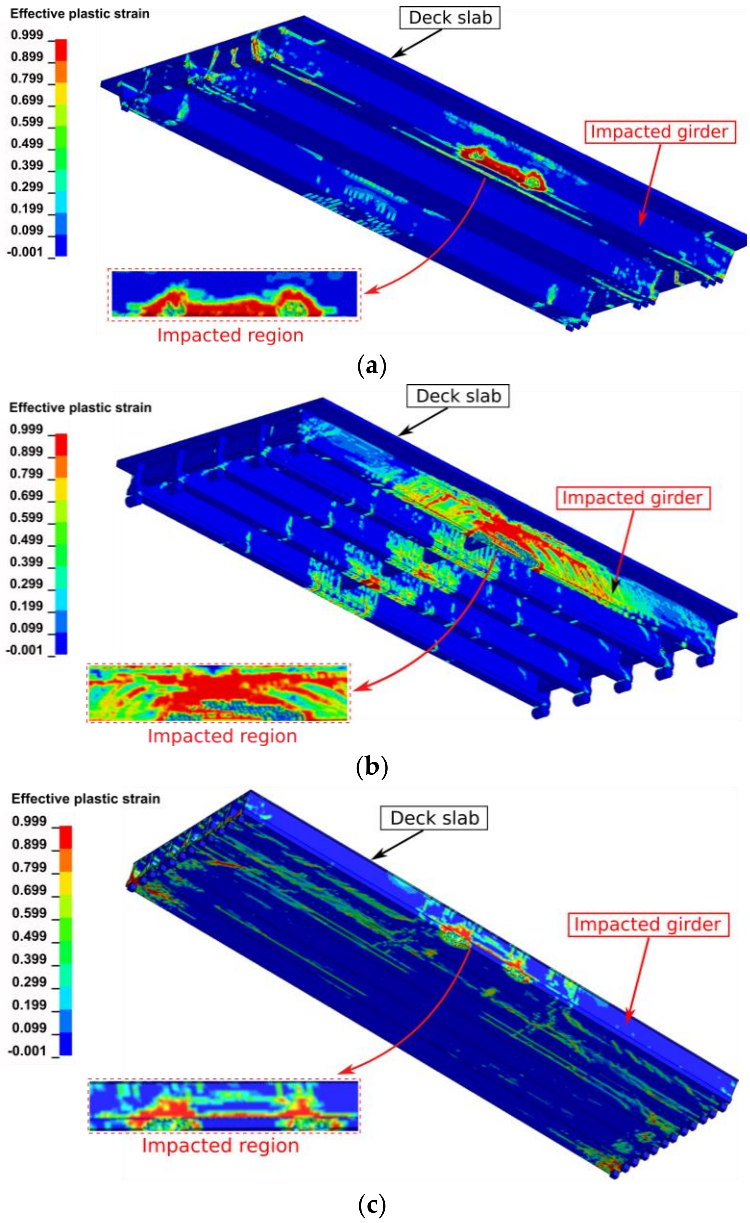

Figure 4. Effective plastic strain distribution on (**a**) box girder bridge, (**b**) T-shaped girder bridge, (**c**) hollow slab bridge.

Figure 4b shows the effective plastic strain diagram of the T-shaped girder bridge. As shown in the figure, extensive plastic damage occurred in the majority region of the impacted girder. Since diaphragms were arranged between each T-shaped girder, the plastic damage also spread to the other four girders through the diaphragms. It is found that a large amount of concrete fell off at the impact region and the "horseshoe" part of each T-shaped girder, with the reinforcement being ruptured as well (see Figure 4b).

Figure 4c shows the effective plastic strain diagram of the hollow slab bridge. As can be seen in the figure, the level of plastic damage of the hollow slab bridges is between that obtained from the above two types of bridges. A certain amount of concrete falls off at the impact region with a small number of steel bars yielding. The extension of the plastic damage area on other girders is smaller than that obtained from the T-shaped girder bridge.

(2) Time history curve of the impact force

Figure 5a shows the time history curves of the horizontal impact force for three types of bridges. As shown in the figure, the peak values of the three impact force curves are similar (roughly 1.3 MN), but the time to reach the peak values for the three types of bridges is different, where the time to reach the maximum impact force of the box girder bridge, T-shaped girder bridge and hollow slab bridge are 0.01 s, 0.02 s and 0.06 s, respectively. Further, one can find in Figure 5a that there are two extreme force values for the T-shaped girder bridge in the period after the peak force but only one extreme force value for the box girder and hollow slab bridge. This phenomenon may be due to the fact that diaphragms in the T-shaped girder bridge can transform more load from the impacted girder to other girders with the loading process being extended.

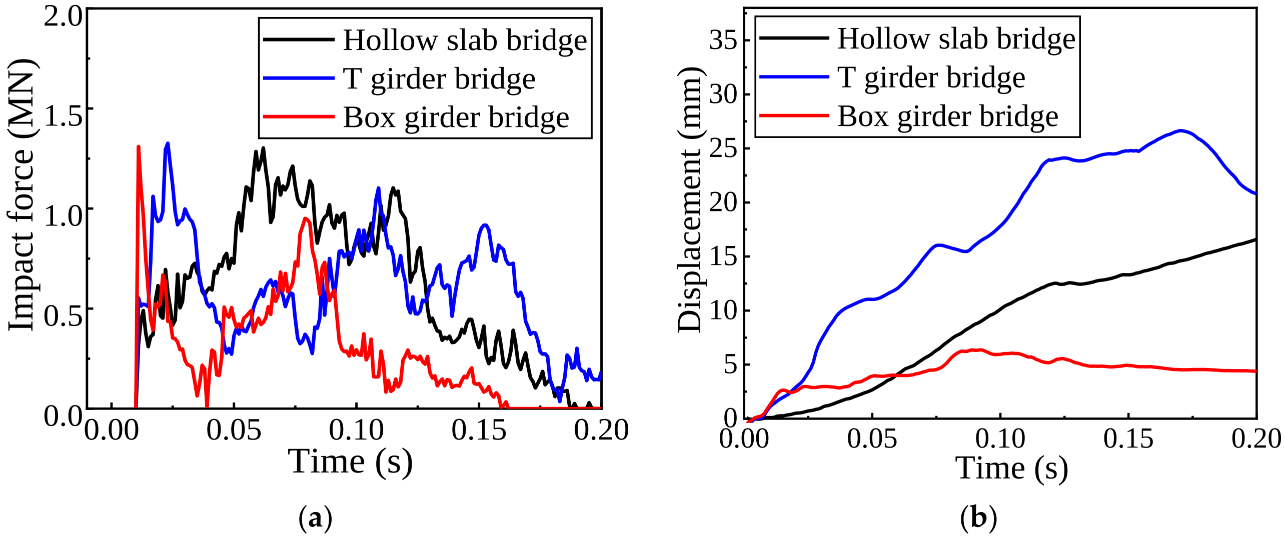

Figure 5. (**a**) Horizontal impact force curves of three types of bridges. (**b**) Midspan displacement curves of three types of bridges.

(3) Time history curve of midspan displacement for three types of bridges

Figure 5b shows the time history curves of displacement obtained at the midspan of the impacted girder for three types of bridges. According to the plastic damage results in Figure 4, one can find that the greater the degree of plastic damage shown on the bridge, the greater the displacement. The maximum displacement of the T-shaped girder bridge, hollow slab bridge and box girder bridge are 27 mm, 17 mm, and 6.3 mm, respectively, whereas the time to reach the maximum displacement for the above three types of bridges is t = 0.175 s, t = 0.2 s and t = 0.1 s, respectively. Further, by analyzing the impact animation, we find that the head of the vehicle starts to lift when the displacement of the bridge reached its maximum value. This phenomenon results in decreased contact between the carriage which further give a rise to a declining trend on both impact force and displacement time history curves.

(4) Summary

The girder configuration has an obvious influence on the local damage and overall displacement of the bridge. Among the investigated three types of bridges, the box girder bridge exhibits the smallest damage during the collision with the displacement at the midspan of the impacted girder being controlled within 7 mm. Whereas the T-shaped girder bridge exhibits the greatest damage during the impact with both local materials at the impact regions and the overall bridge displacement reaching the maximum level. This result implies that the box girder bridge can provide better lateral impact resistance performance in practical engineering.

Further, according to the result in Figure 5a, one can see that the girder configuration has little effect on the maximum impact force generated during the collision, which implies the girder configuration effect can be neglected in the impact force prediction formula for design, which would be discussed in detail in the following Discussion section.

3.2. Influence of the Vehicle Speed on the Dynamic Behavior of the Bridge

The influence of vehicle speed on the dynamic response of the bridge is investigated in this section. In the analysis, the dynamic behavior of the box girder bridge obtained under a vehicle speed of 40 km/h, 60 km/h and 80 km/h is investigated.

(1) Failure mode of the bridge

Figure 6 (v = 40 km/h, 60 km/h) and Figure 4a (v = 80 km/h) show the effective plastic strain distribution on the prestressed concrete box girder bridge obtained under the three investigated impact speeds. As can be seen from the figures, with the vehicle speed increasing, the plastic damage area of the side impacted girder increased as well. When v = 40 km/h, the plastic damage area on the impacted girder is relatively small with only a small amount of concrete falling off from the impact area. When v = 60 km/h, the plastic damage area expands obviously with the concrete at the bottom flange of the girder being further fallen off. When v = 80 km/h (see Figure 4a), the impact area reaches its maximum level. It should be noted no damage was observed at the longitudinal rebars and stirrups at the impact area under the above investigated three vehicle speeds.

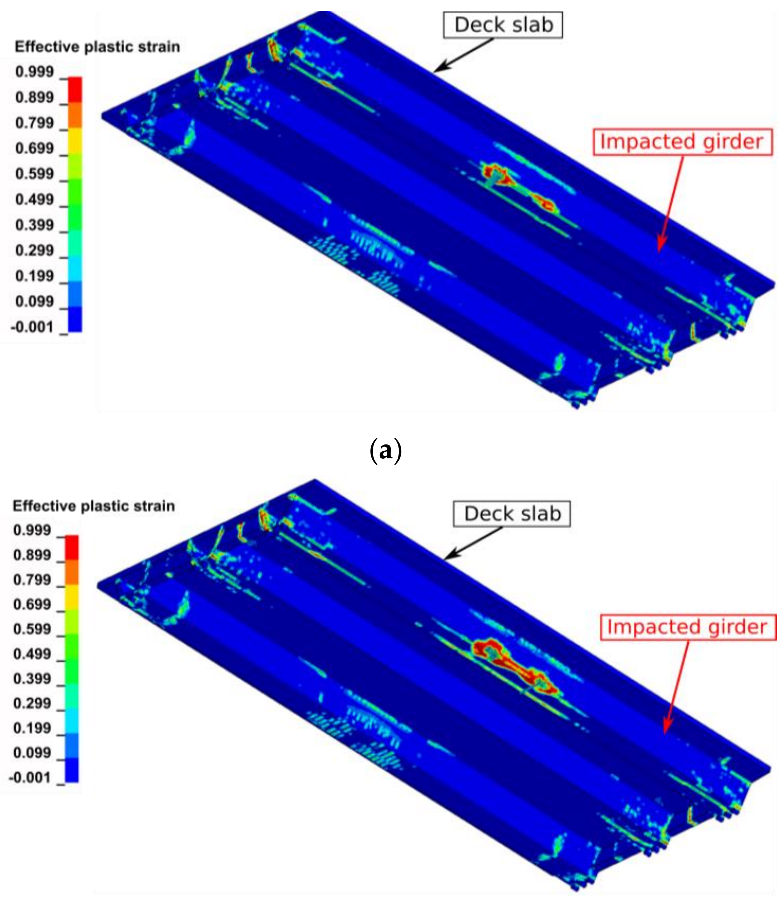

(**a**)

(**b**)

Figure 6. Effective plastic strain distribution on the box girder bridge with the vehicle speed being (**a**) 40 km/h and (**b**) 60 km/h.

(2) Time history curve of the impact force

Both horizontal and vertical impact force time history curves of the PC box girder bridges obtained at different vehicle speeds are shown in Figure 7. According to the results in Figure 7, one can find that the time interval for reaching the maximum impact force continuously shortened and the peak value of the impact force gradually increased as the vehicle speed increased. When the vehicle speed increased from 40 km/h to 80 km/h, the maximum horizontal impact force generated during the collision increased from 0.95 MN to 1.32 MN and the vertical impact force increased from 0.12 MN to 0.18 MN.

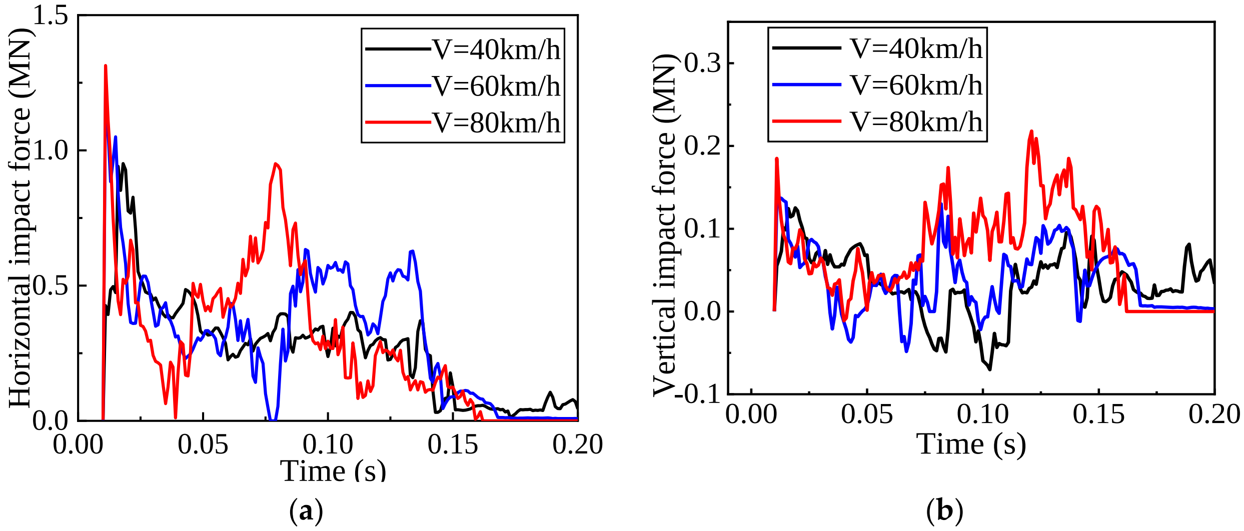

Figure 7. (**a**) Horizontal impact force and (**b**) vertical impact force curve of the PC box girder bridge obtained under different vehicle speeds.

(3) Time history curve of the displacement

The time history curve of displacement obtained at the midspan of the impacted girder under different vehicle speeds is shown in Figure 8. One can find a certain degree of fluctuations can be observed on the three displacement curves. These fluctuations mainly resulted from the relatively low flexural rigidity at the midspan of the bridge. Further, we can find the maximum displacement of the bridge increase with the increase of the vehicle speed. When the vehicle speed increases from 40 km/h to 80 km/h, the maximum displacement obtained at the midspan of the impacted girder increases from 2.5 mm to 6.3 mm.

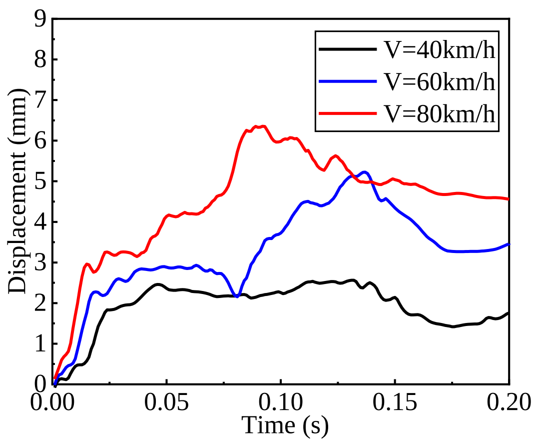

Figure 8. Time history curve of displacement obtained at the midspan of the box girder bridge under different vehicle speeds.

(4) Summary

Vehicle speed has a certain degree of effect on both the local and global response of the PC box girder bridge. With the vehicle speed increasing, the local damage at the impact area, impact force and midspan displacement of the bridge increases.

3.3. Influence of the Vehicle Mass on the Dynamic Behavior of the Bridge

The influence of vehicle mass on the dynamic response of the PC box girder bridge is investigated in this section. Four types of vehicle mass, i.e., 10 tons, 15 tons, 20 tons and 30 tons, are adopted in the collision analysis, with the impact velocity of the vehicle being 80 km/h.

(1) Failure mode of the bridge

Figure 9 (m = 10 t, 15 t and 30 t) and Figure 4a (m = 20 t) show the effective plastic strain distribution on the PC box girder bridge obtained under the four mass conditions. As can be seen in the figures, although the damage at the impact region of the prestressed concrete box girder gradually increases with the increase of the vehicle mass, the damage variation between different mass conditions is not as obvious as that obtained under different vehicle speeds. When the vehicle mass m = 10 t and 15 t, only a small amount of concrete at the impact area of the impacted girder is broken, with no damage showing on the opposite side of the impact girder. When m = 20 t (see Figure 4a) and 30 t, the concrete located at both the impact area and bottom flange of the girder falls off with large plastic damage showing on the opposite side of the impact area.

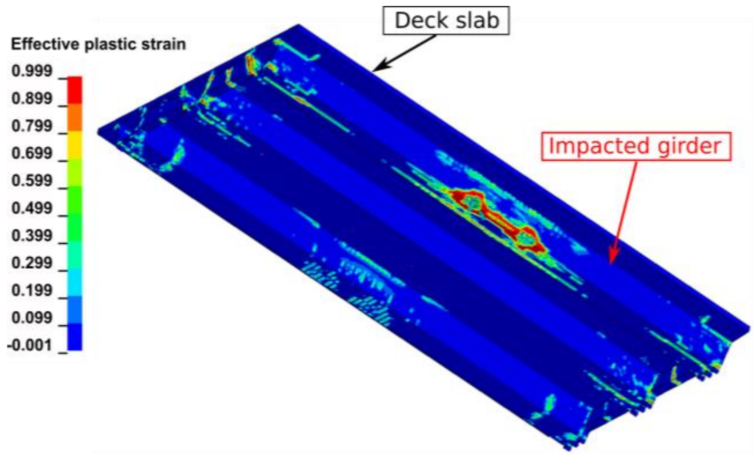

(**a**)

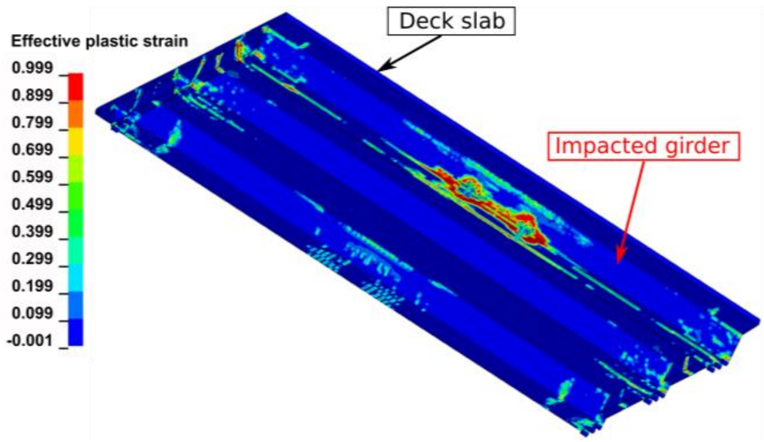

(**b**)

Figure 9. *Cont.*

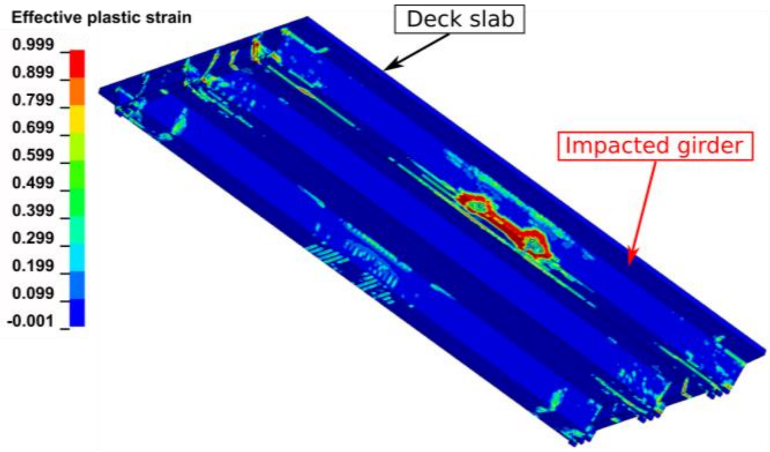

(**c**)

Figure 9. Effective plastic strain distribution on the box girder bridge with the vehicle mass being (**a**) 10 tons, (**b**) 15 tons and (**c**) 30 tons.

(2) Time history curve of the impact force

Figure 10a shows the time history curve of the horizontal impact force of the PC box girder bridge obtained under different vehicle masses. One can see that the four loading curves basically coincide with each other before 0.075 s and then have a different variation trend in the follow-up stage. The peak impact force for four mass conditions (i.e., 10 t, 20 t, 30 t, 40 t) are 1.12 MN, 1.19 MN, 1.22 MN and 1.31 MN, respectively, which indicates the increase of the vehicle mass would increase the impact force of the bridge.

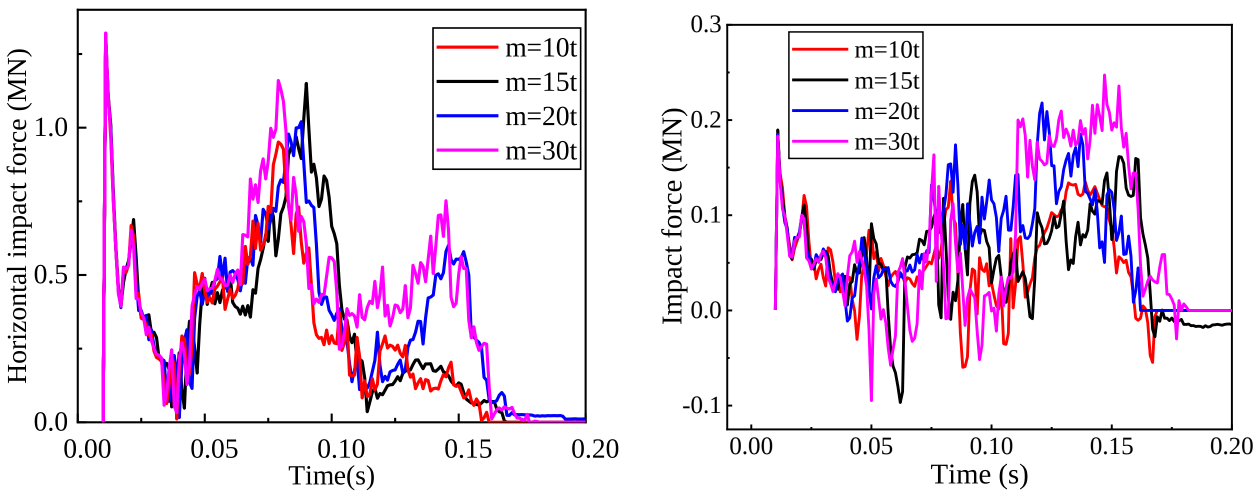

(**a**) (**b**)

Figure 10. (**a**) Horizontal impact force and (**b**) vertical impact force curve of the PC box girder bridge obtained under different vehicle mass conditions.

Figure 10b shows the time history curve of the vertical impact force of the bridge under different vehicle masses. A similar variation manner to the horizontal force is obtained for the vertical impact force, where the vertical impact force gradually increases with the increase of vehicle mass. Meanwhile, with the increase of vehicle mass, the curve fluctuation range increases as well, where the fluctuation values of the four curves are 0.225 MN, 0.228 MN, 0.23 MN and 0.33 MN, respectively.

(3) Time history curve of the displacement

Figure 11 shows the midspan displacement time history curves of the impacted box girder obtained under different vehicle mass conditions. The maximum displacements corresponding to the four different impact masses (i.e., 10 t, 15 t, 20 t and 30 t) are 4.8 mm, 5.8 mm, 6.3 mm and 8.2 mm, respectively, which conforms to the trend that the girder displacement increases with the increase of impact mass.

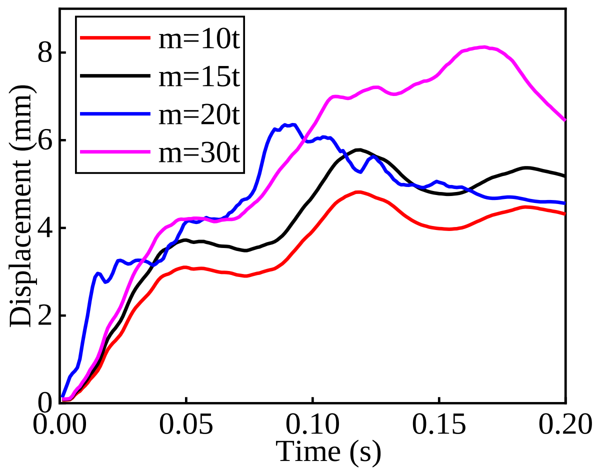

Figure 11. Time history curve of displacement obtained at the midspan of the box girder bridge under different vehicle mass conditions.

(4) Summary

Variation of the vehicle mass is mainly achieved by changing the load capacity of the vehicle carriage. During the impact process, the weight of the vehicle cannot fully act on the superstructure since only a limited area at the top of the carriage collides with the bridge. Further, the head of the vehicle will lift during the collision during the impact process, which would further reduce the impact mass acting on the bridge. Therefore, although the increase of the vehicle mass would increase the local damage, impact force and midspan displacement of the bridge, the influence of this factor on the dynamic response of the bridge is not obvious as that of vehicle speed.

3.4. Influence of the Impact Angle on the Dynamic Behavior of the Bridge

The influence of impact angle (i.e., the angle between the driving direction of the vehicle and the cross-section of the bridge, which is defined as θ, see Figure 1d) on the dynamic response of the prestressed concrete box girder bridge is investigated in this section. Three types of impact angles, i.e., 0°, 15° and 30°, are adopted in the collision analysis.

(1) Failure mode of the bridge

Figure 12 (θ = 15° and 30°) and Figure 4a (θ = 0°) show the plastic strain distribution on the prestressed concrete box girder bridge with the vehicle impact angle being 0°, 15° and 30°, respectively. As shown in the figures, the plastic damage that occurred on the main girder increased obviously with the increase of the impact angle. When the impact angle θ = 0° (see Figure 4a), the concrete at the impact area of the side girder fell off with no damage occurring on the rebars. When θ = 15°, the plastic damage extends to the bottom flange of the girder with the rebars at the bottom flange being ruptured. When θ = 30°, the damage degree on the bridge further increases with more steel bars at the impact area being ruptured. It should be noted, with the impact angle changing, the vehicle would continue to crash on the second girder behind the side girder. This follow-up collision further resulted in plastic damage on other girders (see Figure 12).

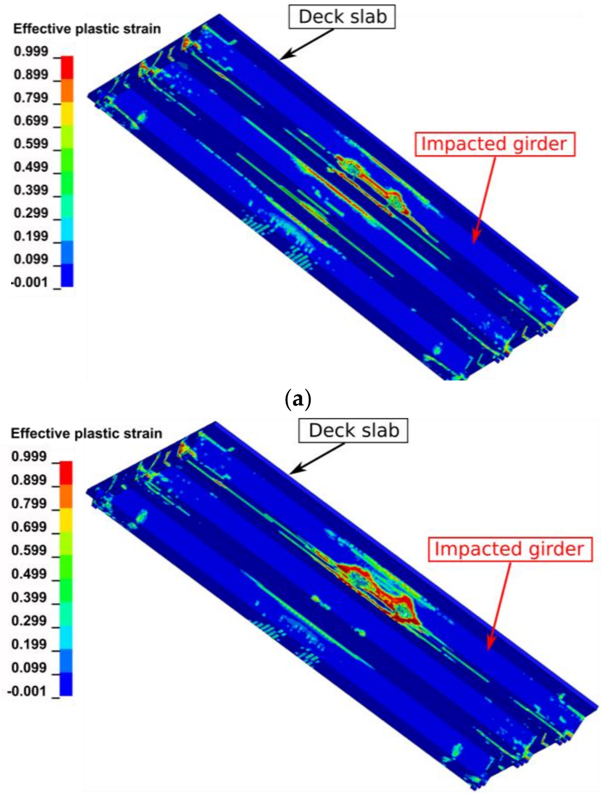

(**a**)

(**b**)

Figure 12. Effective plastic strain distribution on the box girder bridge with the vehicle impact angle being (**a**) 15° and (**b**) 30°.

(2) Time history curve of the impact force

Figure 13a shows the time history curves of the horizontal impact force of the bridge under different impact angles. As can be seen from the figure, the peak value of the horizontal impact force gradually decreases with the increase of the impact angle. The corresponding peak values of the impact force at 0°, 15° and 30° are 1.31 MN, 1.09 MN and 1.05 MN, respectively. Then, the impact force decreases gradually to 0 for the condition of θ = 0°, but increases sharply for the conditions θ = 15° and 30°. Such a phenomenon is mainly caused by a follow-up collision between the vehicle and the second girder.

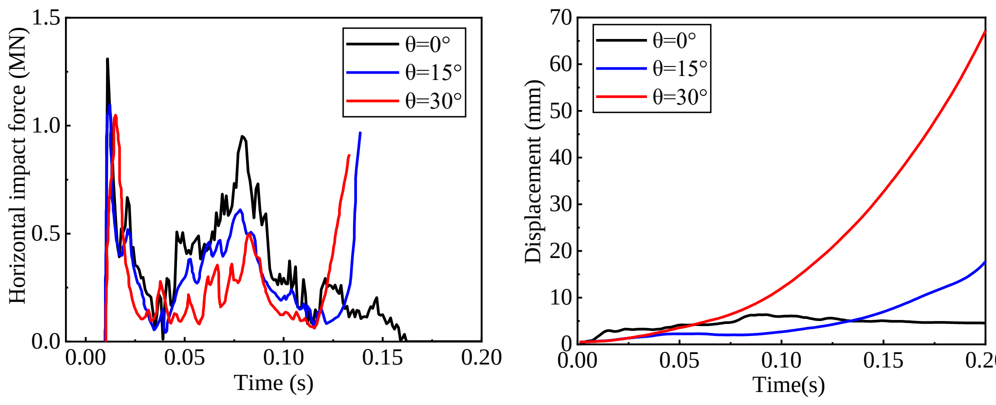

(**a**) (**b**)

Figure 13. (**a**) Horizontal impact force and (**b**) midspan displacement curve of the PC box girder bridge obtained under different impact angles.

(3) Time history curve of the displacement

Figure 13b shows the displacement time history curves of the impacted girder obtained under different impact angles. As shown in Figure 13b, the midspan displacement of the bridge increases sharply with the increase of impact angle. When the impact angle increases from 0° to 30°, the maximum displacement increases from 6.3 mm to 68 mm. Such a phenomenon is caused by the fact that the concrete damage on the opposite side of the impacted girder increased sharply as the impact angle increased.

(4) Summary

The vehicle impact angle has an obvious influence on the local and overall behavior of the bridge. The increase of the impact angle would increase the midspan displacement of the impacted girder and decrease the impact force generated during the collision. Therefore, this influence factor should be considered in the impact force prediction formula (see Section 4).

3.5. Influence of the Concrete Strength on the Dynamic Behavior of the Bridge

The influence of concrete strength on the dynamic response of the PC box girder bridge is investigated in this section. Three types of concrete grade, C40, C50 and C60, are adopted in the collision analysis.

(1) Failure mode of the bridge

Figure 14 (C40 and C60) and Figure 4a (C50) show the effective plastic strain distribution on the prestressed concrete box girder bridge obtained with the concrete grade being C40, C50 and C60. One can find that the concrete strength controls the local plastic damage degree that occurred in the impact area. With the concrete strength increase from C40 to C60, the area of the plastic damage region reduced with the deleted concrete elements at the impact region decreasing from 224 to 68.

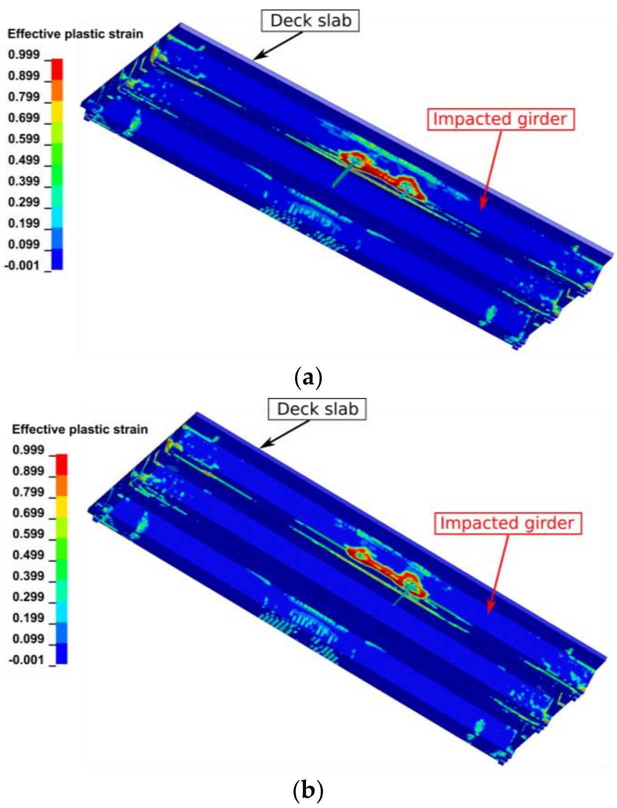

Figure 14. Effective plastic strain distribution on the box girder bridge with the concrete strength being (**a**) C40 and (**b**) C60.

(2) Time history curve of the impact force

Figure 15a shows the time history curve of the horizontal impact force obtained on the prestressed concrete box girder bridge at different concrete strengths. As shown in the figure, the concrete strength has a very limited influence on the impact force curves. Three loading curves almost coincide before t = 0.045 s. The peak values of the impact force under the three working conditions are 1.30 MN, 1.31 MN and 1.32 MN, respectively.

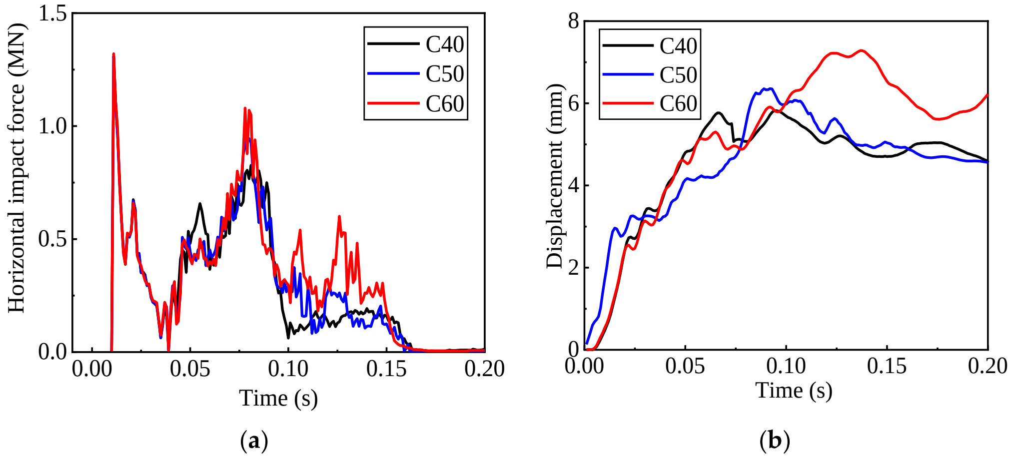

Figure 15. (**a**) Horizontal impact force and (**b**) midspan displacement curve of the PC box girder bridge obtained under different concrete strengths.

(3) Time history curve of the displacement

Figure 15b shows the displacement time history curve of the impacted girder of PC box girder bridges under different concrete strengths. Similar to the horizontal impact curve, the concrete strength has limited influence on the midspan displacement of the bridge. When the concrete strength increases from C40 to C60, the maximum displacement obtained increases from 5.8 mm to 7.8 mm with peak value time gradually moving backward.

(4) Summary

The concrete strength only has a certain influence on the damage of the local vehicle impact region with no obvious effect on the overall dynamic response of the bridge.

3.6. Influence of the Strand Prestress on the Dynamic Behavior of the Bridge

The influence of the strand prestress on the dynamic response of the PC box girder bridge is investigated in this section. Strands having three types of ultimate tensile strength, f_{ptk} = 1860 MPa, 1570 MPa and 1270 MPa, are adopted in the collision analysis, where the prestress of the three investigated strands is equal to 0.75 times its ultimate tensile strength, i.e., 0.75 f_{ptk}.

(1) Failure mode of the bridge

Figure 16 (f_{ptk} = 1270 MPa and 1570 MPa) and Figure 4a (f_{ptk} = 1860 MPa) show the effective plastic strain distribution on the prestressed concrete box girder bridges obtained under different strand prestress conditions. As can be seen in the figure, the plastic damage generated at the impact area decreases with the increase of the strand prestress. When the strand with f_{ptk} = 1270 MPa is adopted, the plastic damage area on the impacted girder is the largest with a large amount of concrete at both the impact area and the bottom flange of the girder falling off and steel bars in the impact area being ruptured. When the strand with f_{ptk} = 1570 MPa is adopted, the plastic damage area becomes smaller, where no fracture occurs on the steel bars in the impact area. When the strand with f_{ptk} = 1870 MPa is adopted, the plastic damage degree at the impact area is the minimum.

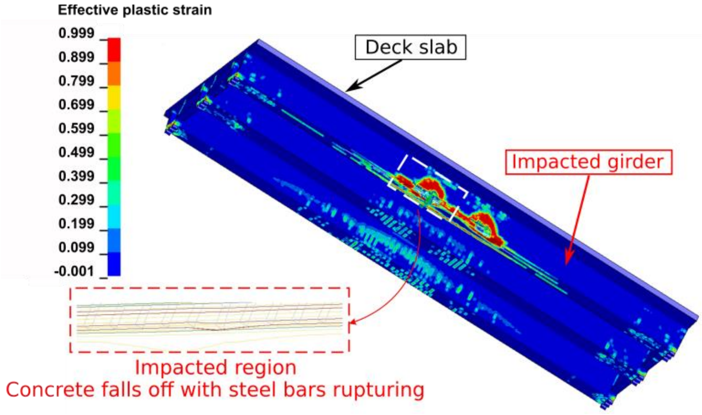

(**a**)

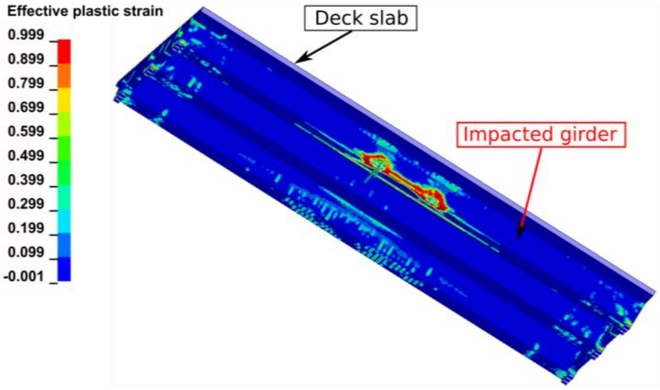

(**b**)

Figure 16. Effective plastic strain distribution on the box girder bridge with the ultimate tensile strength of the strand being (**a**) 1270 MPa and (**b**) 1570 MPa.

(2) Time history curve of the impact force

Figure 17 shows the time history curve of the horizontal impact force of the prestressed concrete box girder bridges obtained under three prestress conditions. As can be seen in the figure, three impact force curves almost coincide before t = 0.075 s with the peak values of three impact forces being equal to 1.32 MN. After t = 0.075 s, the three curves deviated greatly.

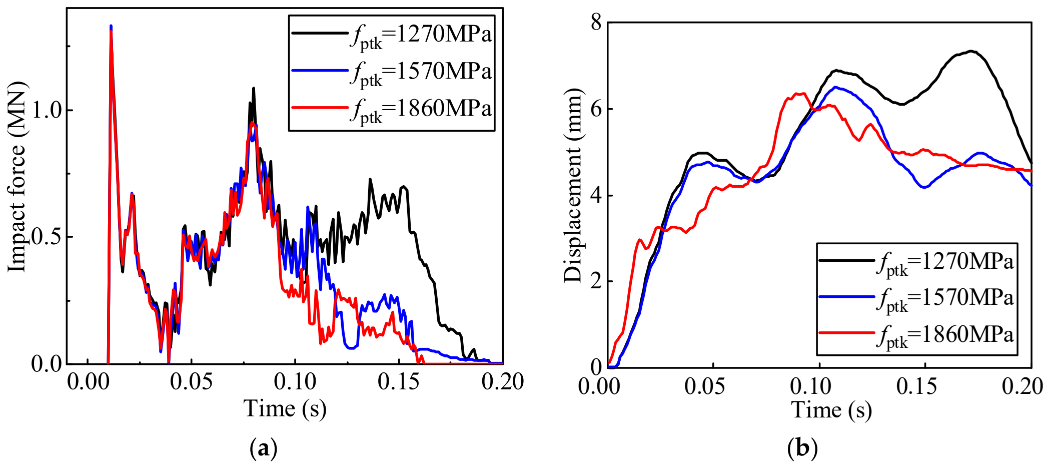

Figure 17. (**a**) Horizontal impact force and (**b**) midspan displacement curve of the PC box girder bridge obtained under different concrete strengths.

(3) Time history curve of the displacement

Figure 17b shows the time history curve of the displacement at the midspan of the impacted girder under different strand prestress. As can be seen in the figure, the maximum value of the midspan displacement of the bridge gradually decreases with the increase of the prestress on the strand. The maximum displacement of the bridge obtained from the three types of strands (f_{ptk} =1270 MPa, 1570 MPa and 1860 MPa) is 7.5 mm, 6.6 mm and 6.3 mm, respectively.

(4) Summary

Similar to the effect of concrete strength, the prestress of the strand only has a certain influence on the damage of the local vehicle impact region with limited effect on the overall dynamic response of the bridge.

4. Impact Force Prediction Formula for PC Box Girder Bridge Subjected to Over-Height Vehicle Collision

The impact force generated from the vehicle collision is a key indicator for assessing the damage degree of the bridge. Therefore, it is essential to establish an accurate prediction formula for impact-induced loading. There are usually two methods to define the impact force generated during a vehicle collision. One method is to use the peak value of the impact force time history F_{peak} as the designed impact force (see Figure 18). Another method is to use the average impact force F_{ave}, defined as the ratio of the total impulse obtained from the time history curve to the impact duration time (see Figure 18), to evaluate the damage degree of the bridge. In this section, both the peak impact force F_{peak} and average impact force F_{ave} for the investigated prestressed concrete box girder bridge are studied. By conducting a parametrical analysis, a quantitative relationship between the two impact force index and corresponding influencing factors are obtained. Then, an empirical prediction formula of vehicle impact force considering multiple influencing factors is established. It should be noted that according to the analysis in Section 3, the horizontal impact force is greater than the vertical impact force, so only the calculation method of the horizontal impact force is investigated in this section.

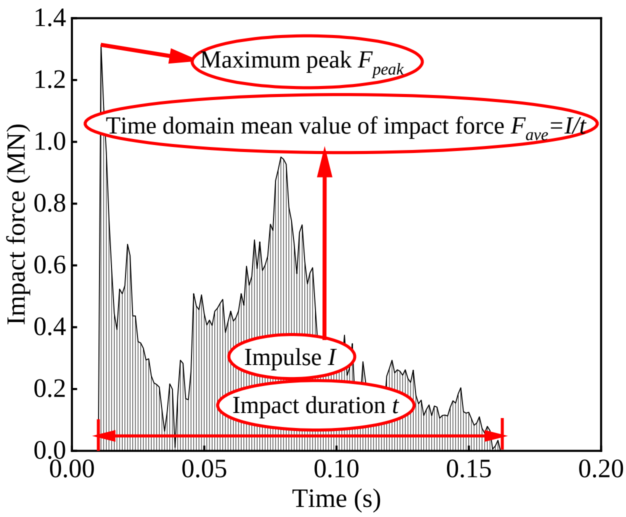

Figure 18. Definition of the peak and average impact force on the impact force time history curve generated during the collision.

4.1. Impact Force Formula Considering Effects of Vehicle Speed and Vehicle Mass

According to the results in Section 3, we can find that the impact force is mainly affected by the vehicle-related factors: i.e., vehicle speed, vehicle mass and impact angle (since the bridge-related parameters, i.e., girder configuration, concrete strength and prestress of the strand, have limited effect on the impact force, these factors are not considered in the impact force formula). To quantitatively establish the relationship between the impact force and the above influence factors, numerical simulations combined with a parametric analysis were conducted on the investigated prestressed concrete box girder bridge. Both the peak and average impact forces under four vehicle mass conditions, i.e., 10 t, 15 t, 20 t and 30 t, and seven vehicle speeds, i.e., 30 km/h, 40 km/h, 50 km/h, 60 km/h, 70 km/h, 80 km/h, 90 km/h, with the vehicle impact angle being 0° were firstly extracted from the analyses. Figures 19 and 20 show the peak and average impact force data obtained from the above-specified conditions, where a nonlinear relationship can be found among the impact force, vehicle mass and vehicle speed. To appropriately reflect such a relationship, inspired by the pioneer's work [23], the following function is developed to estimate the both peak and average impact force

$$F = av^b m^c \tag{8}$$

where F refers to the peak or average impact force, v and m refer to the vehicle speed and mass, a, b and c are three parameters. One can see from Equation (8), the vehicle speed and vehicle mass influence on the impact force are independent of each other and can be characterized by a simple power function. It is worth mentioning, when b = 1.0 and c = 0.5, this impact force formula could degenerate to the hard impact function, i.e., $F = v\sqrt{km}$(k is the stiffness of the impact object), provided in the European Code [19].

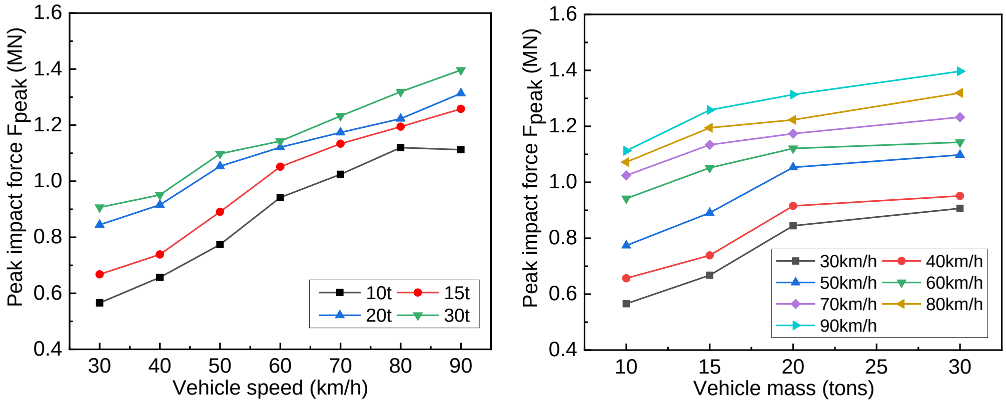

(**a**) (**b**)

Figure 19. The peak impact force data obtained under (**a**) various vehicle speeds and (**b**) various vehicle masses.

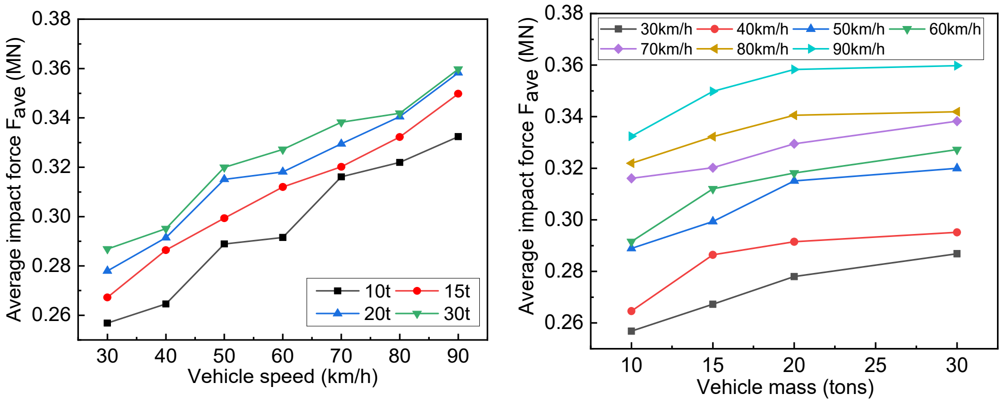

(**a**) (**b**)

Figure 20. The average impact force data obtained under (**a**) various vehicle speeds and (**b**) various vehicle masses.

To calibrate and verify the proposed impact force formula, Equation (8) is used to fit both peak and average impact force data shown in Figures 19 and 20. In the fitting analysis, the values of parameter a, b and c were identified by finding the best-fitting surface of impact force data points through minimizing the average error defined as follows:

$$\Delta = \frac{1}{n}\sum_{i=1}^{n}\left|\frac{F_i - \overline{F}_i}{\overline{F}_i}\right| \tag{9}$$

where Δ is the average error between the fitting surface and the impact force data points, F_i denotes the impact force predicted from Equation (8) and $\overline{F}$ denotes the impact force obtained from the numerical analysis, and n is the number of impact force data points. Figure 21 shows the fitted results from Equation (8) for both peak and average impact force data, where the values of fitted parameters for peak impact force F_{peak} are a = 0.070, b = 0.502 and c = 0.224, and that for average impact force F_{ave} are a = 0.099, b = 0.227 and c = 0.082 (these values are also listed in Table 3). One can see the fitting surface obtained from Equation (8) is in good agreement with both peak and average impact force data points. The predicted average error for the peak and average impact force data points are Δ = 4.8% and 1.1%, respectively, which verifies the good prediction performance of the proposed impact force formula.

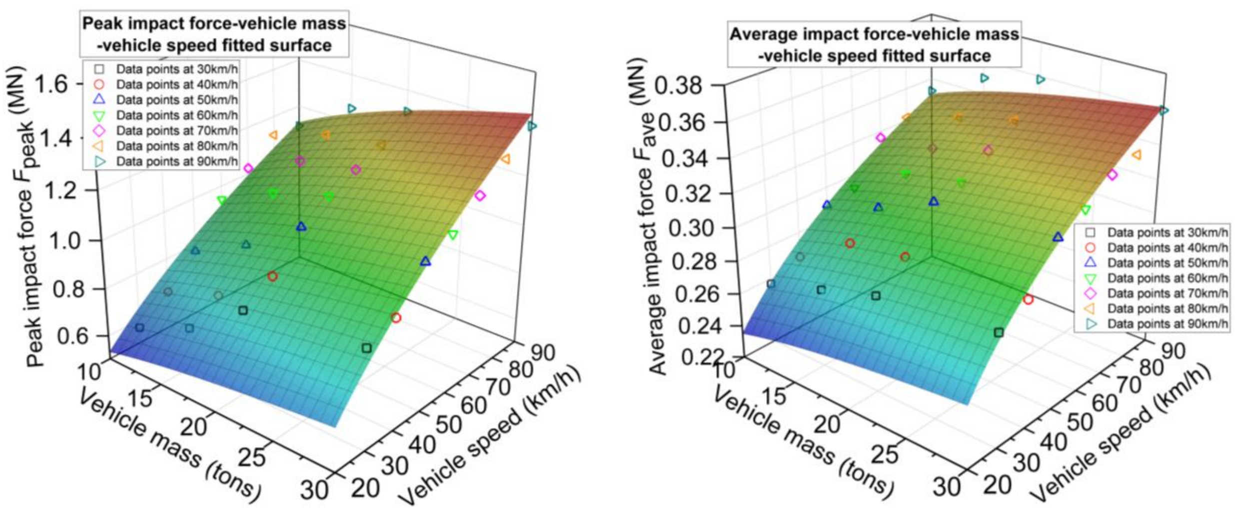

(**a**) (**b**)

Figure 21. The fitted surface from the proposed impact force formula for (**a**) peak impact force data and (**b**) average impact force data obtained under various vehicle masses and speeds.

Table 3. Calibrated parameters in the proposed impact force formula.

Impact Force	Parameters in the Impact Force Formula					
	a	b	c	d	e	f
Peak impact force F_{peak}	0.07	0.502	0.224	−0.377	0.137	0.007
Average impact force F_{ave}	0.099	0.227	0.082	−2.745	2.118	0.044

4.2. *Impact Force Formula Further Accounting for the Effect of Impact Angle*

Although the effect of the vehicle impact angle on the dynamic response of a bridge superstructure was extensively recognized, this factor was not taken into account in the impact force prediction formula in most current research and design codes. To further consider the influence of vehicle impact angle in the impact force formula, corresponding numerical simulation analyses were carried out for the investigated PC box girder bridge. This time, both the peak and average impact force under three vehicle impact angles, i.e., 0°, 15°, 30°, and four vehicle mass conditions, i.e., 10 t, 15 t, 20 t and 30 t, with the vehicle speed being 80 km/h, are extracted from the numerical analyses. Figure 22 shows the peak and average impact force data points obtained under various impact angles. As can be seen from Figure 22, both the peak and average impact force decrease in a nonlinear manner as the impact angle increases. Such a phenomenon is because only a part of the impact force generated in the vehicle's driving direction is transferred to the normal direction of the bridge during the collision.

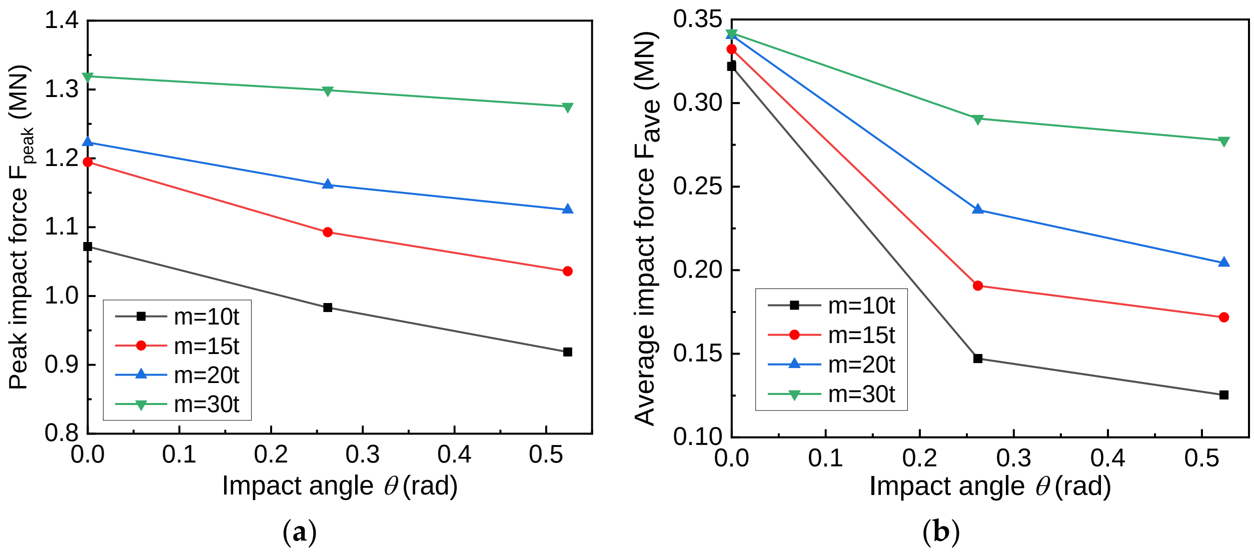

Figure 22. (**a**) The peak impact force data obtained under various impact angles. (**b**) The average impact force data obtained under various impact angles.

To further reflect the influence of the impact angle in the impact force formula, we extended Equation (8) in the following form.

$$F = av^b m^c \left(1 + d\theta + e\theta^2 + fm\theta\right) \tag{10}$$

where θ is the impact angle of the vehicle, d, e and f are three parameters. As it can be seen in Equation (10), an impact angle influence term, expressed as a quadratic function of the impact angle, is added in the original Equation (8) to characterize impact angle influence. It should be noted, when the impact angle θ = 0°, Equation (10) degenerates to Equation (8), which ensures the consistency of the two equations.

To further calibrate and verify the extended impact force formula, Equation (10) is used to fit both peak and average impact force data shown in Figure 22. Since the values of parameters a, b and c were already calibrated based on the data in the previous Section 4.1 (see Table 3), only the parameters d, e and f are determined in the fitting analysis this time. Figure 23 shows the fitted result from Equation (10) for both peak and average impact force data under various impact angles, where the values of fitted parameters for peak impact force F_{peak} are $d = -0.377$, $e = 0.137$ and $f = 0.007$, and those for average impact force F_{ave} are $d = -2.745$, $e = 2.118$ and $f = 0.044$ (also listed in Table 3). One can see in Figure 23 that the fitted surfaces obtained from Equation (10) agree well with both peak and average impact force data points. The predicted average error from Equation (10) for the peak and average impact force data points are $\Delta = 0.9\%$ and 4.5%, respectively, which verifies the prediction performance of the developed impact force formula.

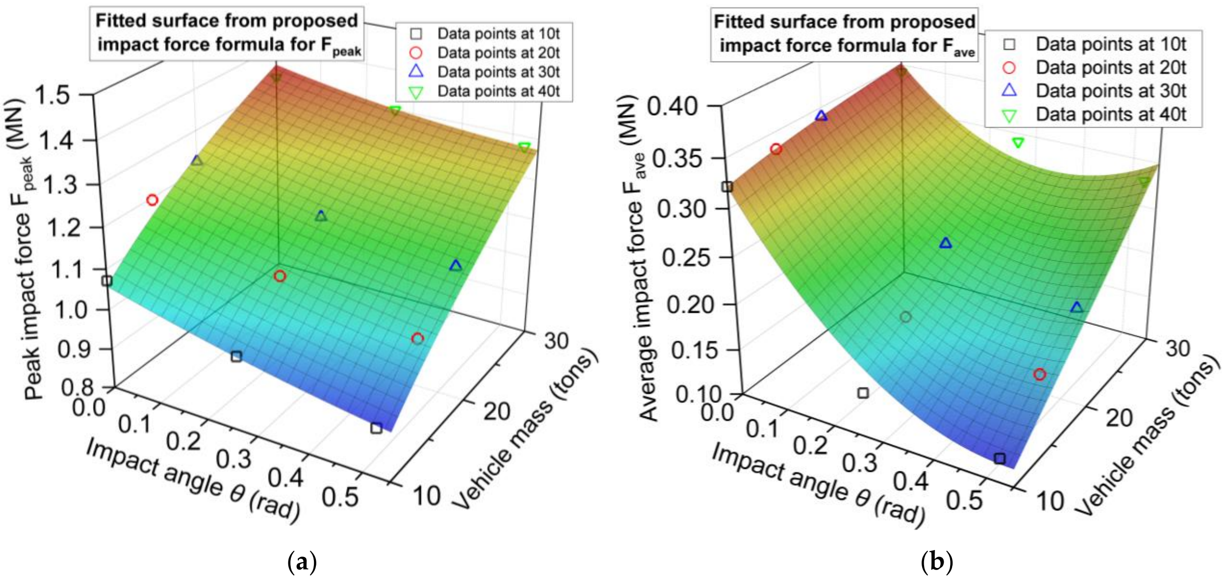

Figure 23. The fitted surface from the proposed impact force formula for (**a**) peak impact force data and (**b**) average impact force data obtained under various vehicle masses and impact angles.

5. Discussion

A few research works were carried out in the literature to identify the potential influencing factors on the impact force generated from the over-height vehicle to bridge collision. Xu et al. [20] studied the collision mechanism between the over-height vehicle and different types of bridges using numerical simulation methods. The numerical results show that the vehicle-related parameters, e.g., vehicle speed, had more influence than the bridge-related parameters, i.e., the bridge type, number of spans, and support conditions, on the impact force. Berton et al. [34] used a simplified finite element model to evaluate the influence of vehicle mass, vehicle speed, bridge deck mass and stiffness on the dynamic behavior of the bridge, which indicates the impact force is proportional to the vehicle speed, mass, and bridge deck stiffness. Kong et al. [22] analyzed the damage of the PC box girder bridge subject to a vehicle collision via finite element analyses. The FE analyses show that the collision force was influenced by the vehicle speed, mass, impact height, and carriage thickness. Oppong et al. [23] studied the influences of different types of impacting objects on the bridge superstructure through a refined FE model and developed a set of impact force prediction equations as a function of impact velocity, impact area, and the dimension of the impacting object. According to the results of this study, we can find that the impact force transferred to the bridge superstructure during the vehicle collision is mainly controlled by the vehicle-related parameters, whereas the bridge-related parameters, i.e., girder configuration, concrete strength and prestress of the strand, illustrate a very limited effect on it. This result was similar to that obtained from Refs. [20,22,23]. The reason for such a phenomenon is that the weight and stiffness of most bridge superstructures are far greater than those of over-height vehicles. As a result, the collision between the vehicle and bridge superstructure is more like a hard impact condition, in which most of the energy and deformation is mainly dissipated by the impacted vehicles. In this context, for a bridge superstructure with a similar weight and stiffness, it seems that we can use a general impact force formula to estimate the impact force generated during the collision.

Compared with other impact force prediction methods for an over-height vehicle collision in the literature, the impact force formula proposed in this study has some advantages: (1) The formula in this study provides a general form for impact force calculation with the majority of vehicle-related parameters being considered. This formula can also degenerate into the simple hard impact force design formula provided in the European code [19]. For different types of bridges and vehicles, researchers can directly calibrate the parameters of the proposed formula using corresponding experimental or numerical data and calculate the corresponding reference impact force for design. (2) The impact force formula in this study further accounts for the influence of impact angle, which is generally not considered in other research. This extends the scope of the current impact design methods. (3) The proposed impact formula can be used to provide reference impact force values for designing a PC box girder bridge subjected to a two-axle truck collision. According to the data in Table 3 and Equation (10), for a regular two-axle truck, the peak and average impact force transferred to the PC box girder bridge under a vehicle velocity of 30 km/h~80 km/h are in the range of 650~1360 kN and 260~350 kN.

In addition, it should be noted, as well as the influence factors investigated in this study, other parameters, such as the traffic condition and vertical clearance, etc. [16], may also affect the impact force during the collision. In this context, more research is needed to expose the influence of these underlying factors. Finally, the impact force formula proposed in this study should be also verified by more follow-up research data.

6. Conclusions

The dynamic response of the prestressed concrete box girder bridge subject to the over-height vehicle collision is studied using the finite element analysis software LS-DYNA. A parametric analysis is conducted to investigate the effects of different influence factors on both local damage and the overall performance of the bridge. Further, a formula for predicting the peak and average impact force of the prestressed concrete box girder bridge impacted by the over-height vehicle is developed. The main conclusions are summarized as follows:

(1) The girder configuration has an obvious influence on the local damage and overall displacement of the bridge. Among the investigated three types of bridges, the box girder bridge exhibits the smallest damage during the collision, whereas the T-shaped girder bridge exhibits the greatest damage, which indicates that the box girder bridge can provide better lateral impact resistance in practical engineering.

(2) The vehicle speed, vehicle mass and impact angle have obvious effects on both local damage and the overall displacement of the PC box girder bridge. With the vehicle speed, mass and impact angle increasing, the local damage and midspan displacement of the PC box girder bridge increased.

(3) The concrete strength and prestress of the strand only have a certain effect on the local damage at the impact area with very limited influence on the overall behavior of the bridge.

(4) The impact force transferred to the bridge superstructure during the vehicle collision is mainly controlled by the vehicle-related parameters, whereas the bridge-related parameters illustrate a very limited effect on it. The peak and average impact force induced by the investigated truck having a mass of 10–30 tons at speeds between 30 km/h and 80 km/h were in the range of 650~1360 kN and 260~350 kN.

(5) The proposed impact force formula comprehensively accounts for the influence of the vehicle speed, vehicle mass and impact angle and can accurately predict the peak and average impact force generated under different working conditions, which provides a method for the impact resistant design of the PC box girder bridge.

Author Contributions: Conceptualization, Y.J.; methodology, Y.Z. (Yongjun Zhou) and Y.Z. (Yu Zhao); software, X.Z.; validation, Y.J. and X.Z.; formal analysis, X.Z.; data curation, X.Z. and Y.J.; writing—original draft preparation, X.Z.; writing—review and editing, Y.J. and W.L.; visualization, X.Z. and W.L.; supervision, Y.Z. (Yongjun Zhou) and Y.Z. (Yu Zhao). All authors have read and agreed to the published version of the manuscript.

Funding: This research was funded by the National Natural Science Foundation of China (grant No. 51908049), Natural Science Basic Research Plan in Shaanxi Province of China (grant No. 2019JQ-677).

Institutional Review Board Statement: Not applicable.

Informed Consent Statement: Not applicable.

Data Availability Statement: Not applicable.

Conflicts of Interest: The authors declare no conflict of interest.

Nomenclature

CDIF	compressive dynamic increase factor
TDIF	tensile dynamic increase factor
f_{cd}	dynamic compressive strength at the strain rate $\dot{\varepsilon}_d$
f_{cs}	static compressive strength at the strain rate $\dot{\varepsilon}_{cs}$
f_{td}	dynamic tensile strength at the strain rate $\dot{\varepsilon}_d$
f_{ts}	static tensile strength at the strain rate $\dot{\varepsilon}_{ts}$
f_{c0}	reference concrete strength
$\dot{\varepsilon}_{cs}$, $\dot{\varepsilon}_{ts}$	reference strain rates
$\dot{\varepsilon}_d$	the strain rate of the concrete
$\alpha, \beta, \gamma, \delta$	parameters corresponding to compressive and tensile dynamic increase factor
σ_{y}	yield stress
ε	the strain rate of the steel
C, P	strain rate coefficients in the Cowper-Symonds model
σ_0	initial yield stress of reinforcement
η	a parameter used to adjust equivalent strengthening
ε^p_{eff}	equivalent plastic strain of the reinforcement
E	Young's modulus
E_t	tangent modulus
E_p	plastic hardening modulus
ΔT	cooling temperature value
N	effective preload applied on the prestressed strand
A	cross-sectional area of the prestressed strand
φ	linear expansion coefficient
F_{peak}	peak impact force
F_{ave}	average impact force
F	impact force
v	vehicle speed
m	vehicle mass
θ	impact angle of the vehicle
a, b, c, d, e, f	parameters in the proposed impact force formula

References

1. Wang, J.H.; Ye, X.Y. Application of laser collision avoidance system for viaduct [N/OL]. *Beijing Evening*. 31 July 2007. Available online: http://news.sina.com.cn/c/2007-07-31/143012303005s.shtml (accessed on 30 December 2022).
2. Nguyen, B.; Brilakis, I. Understanding the problem of bridge and tunnel strikes caused by over-height vehicles. *Transport. Res. Rec.* **2016**, *14*, 3915–3924. [CrossRef]
3. Nguyen, B. Vision-Based Over-Height Vehicle Detection for Warning Drivers. Ph.D. Thesis, University of Cambridge, Cambridge, UK, 2018.
4. Feldman, L.R.; Jirsa, J.O.; Kowal, E.S. Repair of bridge impact damage. *Concr. Int.* **1998**, *20*, 61–66.
5. Fu, C.C.; Burhouse, J.R.; Chang, G.L. Overheight vehicle collisions with highway bridges. *Transport. Res. Rec.* **2004**, *1865*, 80–88. [CrossRef]
6. Fujikake, K.; Li, B.; Soeun, S. Impact response of reinforced concrete beam and its analytical evaluation. *J. Struct. Eng.* **2009**, *135*, 938–950. [CrossRef]
7. Kishi, N.; Mikami, H.; Matsuoka, K.; Ando, T. Impact behavior of shear-failure-type RC beams without shear rebar. *Int. J. Impact Eng.* **2002**, *27*, 955–968. [CrossRef]
8. Jin, L.; Lan, Y.C.; Zhang, R.B.; Du, X.L. Impact resistance of RC beams under different combinations of mass and velocity: Mesoscale numerical analysis. *Arch. Civ. Mech. Eng.* **2020**, *20*, 119–125. [CrossRef]
9. Xu, L.J.; Lu, X.Z.; Smith, S.T.; He, S.T. Scaled model test for collision between over-height truck and bridge superstructure. *Int. J. Impact Eng.* **2012**, *49*, 31–42. [CrossRef]
10. Jing, Y.; Ma, Z.J.; Clarke, D.B. Full-scale lateral impact testing of prestressed concrete girder. *Struct. Concr.* **2016**, *17*, 947–958. [CrossRef]

11. Huang, Z.; Chen, W.; Tran, T.T.; Pham, T.M.; Hao, H.; Chen, Z.; Elchalakani, M. Experimental and numerical study on concrete beams reinforced with basalt FRP bars under static and impact loads. *Compos. Struct.* **2021**, *263*, 113648. [CrossRef]
12. Nghiem, A.; Kang, H. Drop-weight testing on concrete beams and ACI design equations for maximum and residual deflections under low-velocity impact. *ACI struct. J.* **2020**, *117*, 199–210.
13. Yang, M.; Qiao, P.; McLean, D.I.; Khaleghi, B. Effects of Overheight Truck Impacts on Intermediate Diaphragms in Prestressed Concrete Bridge Girders. *PCI J.* **2010**, *55*, 58–78. [CrossRef]
14. Zhang, J.F.; Wang, R.; Zhang, Z.C.; Tong, C.K.; Zhang, Y. Residual performance and damage mechanism of prestressed concrete box girder bridge subjected to falling heavy object impact. *Struct. Infrastruct. Eng.* **2022**, 2035775. [CrossRef]
15. Cao, R.; Agrawal, A.K.; El-Tawil, S.; Wong, W. Overheight impact on bridges: A computational case study of the Skagit River bridge collapse. *Eng. Struct.* **2021**, *237*, 112215. [CrossRef]
16. Das, S.; Brenkus, N.R.; Tatar, J. Strategies for prevention, protection, and repair of bridge girders vulnerable to over-height vehicle impacts: A state-of-the-art review. *Structures* **2022**, *44*, 514–533. [CrossRef]
17. Ministry of Transport of the People's Republic of China. *General Specifications for Design of Highway Bridges and Culverts JTG D60-2015*; People's Communications Press: Beijing, China, 2015. (In Chinese)
18. American Association of State Highway Transportation Officials. *AASHTO LRFD Bridge Design Specifications*, 8th ed.; American Association of State Highway Transportation Officials: Washington, DC, USA, 2017.
19. *EN 1991-1-7*; Eurocode 1: Actions on Structures-Part 1-7: General Actions-Accidental Actions. The European Union: Brussels Belgium, 2006.
20. Xu, L.J.; Lu, X.Z.; Guan, H.; Zhang, Y.S. Finite element and simplified models for collision simulation between overheight trucks and bridge superstructures. *J. Bridge Eng.* **2013**, *18*, 1140–1151. [CrossRef]
21. Liu, X.Y.; Zhu, Z.Z.; Jiang, T.X.; Chen, C.P. Simulation analysis and research on impact force of impacted bridge structure. *J. Hunan Ins. Tech.* **2015**, *28*, 63–68. (In Chinese)
22. Kong, L.; Zhang, J.; Han, W. Investigation on damage and simplified collision force of prestressed concrete box bridge subjected to over-height truck collision. In Proceedings of the 2020 International Conference on Intelligent Transportation, Big Data & Smart City (ICITBS), Vientiane, Laos, 11–12 January 2020; IEEE: Piscataway Township, NJ, USA, 2020.
23. Oppong, K.; Saini, D.; Shafei, B. Characterization of impact-induced forced and damage to bridge superstructures due to over-height collision. *Eng. Struct.* **2021**, *236*, 112014. [CrossRef]
24. Livermore Software Technology Corporation. *LS-DYNA Keyword User's Manual R8.0*; Livermore Software Technology Corporation: San Francisco, CA, USA, 2015.
25. Hao, Y.F.; Hao, H. Influence of the concrete DIF model on the numerical predictions of RC wall responses to blast loadings. *Eng. Struct.* **2014**, *73*, 24–38. [CrossRef]
26. Chen, W.; Hao, H.; Chen, S. Numerical analysis of prestressed reinforced concrete beam subjected to blast loading. *Mater. Des.* **2015**, *65*, 662–674. [CrossRef]
27. Jiang, H.; Chorzepa, M.G. An effective numerical simulation methodology to predict the impact response of pre-stressed concrete members. *Eng. Fail. Anal.* **2015**, *55*, 63–78. [CrossRef]
28. NCAC. Finite Element Model Archive [EB/OL]. (2010-12-21). Available online: http://thyme.ornl.gov/FHWA/F800WebPage/description/description.html (accessed on 10 July 2021).
29. Mohan, P.; Marzougui, D.; Kan, C.D. Validation of a Single Unit Truck model for roadside hardware impact. *Int. J. Veh. Syst. Model. Test.* **2007**, *2*, 1. [CrossRef]
30. Sharma, H.; Hurlebaus, S.; Gardoni, P. Performance-based response evaluation of reinforced concrete columns subject to vehicle impact. *Int. J. Impact Eng.* **2012**, *43*, 52–62. [CrossRef]
31. Do, T.V.; Pham, T.M.; Hao, H. Dynamic responses and failure modes of bridge columns under vehicle collision. *Eng. Struct.* **2017**, *156*, 243–259. [CrossRef]
32. El-Tawil, S.; Severino, E.; Fonseca, P. Vehicle Collision with Bridge Piers. *J. Bridge Eng.* **2005**, *10*, 345–353. [CrossRef]
33. Hu, C.M.; Han, L.H.; Hou, C.C. Concrete-encased CFST Members with Circular Sections under Laterally Low Velocity Impact: Analytical Behavior. *J. Constr. Steel Res.* **2018**, *146*, 135–154. [CrossRef]
34. Berton, E.; Bouaanani, N.; Lamarche, C.P.; Roy, N. Finite element modeling of the impact of heavy vehicles on highway and pedestrian bridge decks. *Procedia Eng.* **2017**, *199*, 2451–2456. [CrossRef]